INFN Istituto Nazionale di Fisica Nucleare
LABORATORI NAZIONALI DI FRASCATI
SIS – Pubblicazioni

LNF-06/04 (P)
February 9, 2006

STATISTICAL MODEL OF SPHALERITE STRUCTURED QUATERNARY $A_{1-X}B_XY_YZ_{1-Y}$ SYSTEMS

B.V. Robouch[*a], A. Kisiel[b], A. Marcelli[a], M. Cestelli Guidi[a], M. Piccinini[a], E. Burattini[c], A. Mycielski[d]

[a] *INFN-Laboratori Nazionali di Frascati Via E. Fermi 40, I-00044 Frascati, Italy*
[b] *Instytut Fizyki, Universytet Jagiellonski, Reymonta 4, 30-059 Krakow, Poland*
[c] *University of Verona, Department of Informatics, strada LeGrazie 15, I-37134 Verona, Italy*
[d] *Instytut Fizyki PAN, Al. Lotnikow 32/46 Warszawa, Poland*

Abstract

Tetrahedron coordinated sphalerite quaternary systems of type $A_{1-x}B_xY_yZ_{1-y}$ consist exclusively of binary and ternary elemental tetrahedra, four of the first and four of the latter, each one with three configurations, i.e., a total of sixteen elemental tetrahedron configurations. These configurations cannot contain all four constituent atoms simultaneously in the same elemental tetrahedron; as a consequence we can consider each ternary tetrahedron composition as diluted in the quaternary compound. Thus, $A_{1-x}B_xY_yZ_{1-y}$ extended x-ray absorption fine structure (EXAFS) data can be treated by using the *strained tetrahedron* model which, originally developed to deal with ternary systems, has already exhibited excellent agreement with numerous experimental data. To determine ion site occupation preferences of quaternary systems, we applied this model to our EXAFS data for $Cd_{1-x}Mn_xSe_yTe_{1-y}$ and to $Ga_xIn_{1-x}As_ySb_{1-y}$ data available in the literature, and compared them to those derived from ternary data for $Cd_{1-x}Mn_xTe$ and $Ga_xIn_{1-x}As$. In both sets, as the ternary is diluted in the quaternary system, a drift of the preference values of the pure ternary is observed. The present analysis of experimental reflectivity far infrared (FIR) phonon spectra of quaternary $Cd_{1-x}Mn_xSe_yTe_{1-y}$ crystals confirms the model predictions and leads to an interpretation of the experimental data for $A_{1-x}B_xY_yZ_{1-y}$ quaternary systems.

PACS.: 61.43 Dq

Accepted
Journal of Alloys and Compounds (in press)

1. Introduction

In recent years, interest in multinary semiconductors has developed rapidly, moving from binary to ternary, then to quaternary systems. The evolution is due to the fact that an extra ion-component leads to an additional degree of freedom in controlling material parameters. Indeed, cation substitution in a sublattice of a matrix of cations, and in the other sublattice an anion by another anion, causes continuous reconstruction of the electronic structure and the phonon spectra as the composition varies, leading to unique property variations. As observed, the ion substitution exhibits site occupation preferences (SOPs) linked to the thermodynamic properties of the creation of the quaternary system.

We symbolise cations by A, B, C, anions by X, Y, Z, and the relative contents of site competing ions by *x* for cations by *y* for anions. We recall here that the elemental structure of a sphalerite (zincblende) binary AZ is a regular tetrahedron with alternatively at the centre an A (or a Z) ion, and at its four vertexes the other Z (or A) ion. Alloying two binary systems such as AZ + BZ (or AZ+AY) leads to the formation of different ternary $A_{1-x}B_xZ$ (or AY_yZ_{1-y}) systems with A ions being progressively substituted by B ions (or Z by Y). Thus, one of the sublattices remains homogeneously mono-ion, while the other is modulated by the two competing ions. At the same time the tetrahedron is distorted, becoming a strained tetrahedron (see Fig.1 in [1]), whence the name of *strained tetrahedron* model introduced to treat these systems. Further we have the quaternary systems, either $A_{1-x}B_xY_yZ_{1-y}$ (2 cations +2 anions, referred to as Q22), or $A_{1-x-x'}B_x{\cdot}C_xZ$ or $AX_yY_y{\cdot}Z_{1-y-y'}$, systems with respectively 3 cations and 1 anion, or 1 cation and 3 anions (we refer to them respectively as Q31 and Q13).

We thus see that *configuration-structure-wise* the quaternary systems are of two types: the first are the quaternaries of the *unbalanced*, *truly quaternary* type with a 3:1 or 1:3 cation:anion ratio, $A_{1-x-x'}B_x{\cdot}C_xZ$ or $AX_yY_y{\cdot}Z_{1-y-y'}$. Here, of the possible *fifteen* elemental tetrahedron configurations, ion-occupation-wise, three are binary, nine ternary, and three quaternary, as the elementary tetrahedron contains respectively two, three, and four different ions. We shall refer to them respectively as Q31 and Q13 systems. The other type of quaternary is the *balanced* type, with 2 cations and 2 anions, type $A_{1-x}B_xY_yZ_{1-y}$, and can be considered as *pseudo-quaternary* because, of the possible *sixteen* tetrahedron configurations, ion-occupation-wise, four are binary and twelve ternary, while none of their sphalerite tetrahedron configurations can canonically be *quaternary*, i.e., contain four distinct types of ions per tetrahedron (which would imply an antisite occupation point defect). This means that we can consider each ternary constituent with its tetrahedron configuration as being dissolved in the quaternary medium, with $A_{1-x}B_xY_yZ_{1-y}$ consisting of $A_{1-x}B_xY$ or AY_yZ_{1-y}, $A_{1-x}B_xZ$ or BY_yZ_{1-y} and we shall refer to such a quaternary system as a Q22 alloy.

Although all the types of alloys introduced above, e.g., Q31, Q13 and Q22, are usually *chemically* referred to as quaternaries, there is a basic structural difference between the pseudo and the truly quaternary systems. Indeed, while in a truly quaternary system one of its sublattices has a homogeneously mono-ionic population, the complementary sublattice is modulated by the three ion species competing for each site. This leads to a crystal structure with alternatively a homogenous ion shell, followed by a heterogeneous shell with site-competing ions. On the other hand, in pseudo-quaternaries the sublattices, and hence the successive ion

shells, are all heterogeneous, each shell composed alternatively of two anions or of two cations, competing with each other for site occupation in that shell. While the denomination is a consequence of the configuration limitations, it is the existence or not of alternative homogeneous\inhomogeneous shell structures that strongly affects the properties of the two classes of quaternaries.

In the present article we do not address the two *unbalanced* truly quaternary types, but concentrate exclusively on the *balanced* pseudo-quaternary Q22 type of system. Indeed, the strained tetrahedron model designed to treat ternary systems is suitable for interpreting $A_{1-x}B_xY_yZ_{1-y}$ extended x-ray absorption fine structure (EXAFS) data. Thus, the analysis of the constituent ternaries is at the basis of understanding pseudo-quaternary system behaviour and, in particular, their cation-anion SOPs.

The local structures of multinary systems can be investigated using several different techniques, such as neutron scattering, EXAFS or far infrared (FIR) vibrational spectroscopy. Particularly the last two methods yield information on ternary tetrahedron coordinated systems, $A_{1-x}B_xZ$ and AY_yZ_{1-y} type, as well as on both *unbalanced* quaternary systems $A_{1-x-x'}B_{x'}C_xZ$ or $AX_yY_{y'}Z_{1-y-y'}$ (such as CdHgMnTe [2], ZnCdHgTe [3]) and *balanced* quaternaries of type $A_{1-x}B_xY_yZ_{1-y}$ (such as $Cd_{1-x}Mn_xSe_yTe_{1-y}$ [4], $Ga_xIn_{1-x}As_ySb_{1-y}$ [5], $Zn_{1-x}Cd_xSe_yTe_{1-y}$ [6]). However, all the methods allow one to obtain information about the real local structure and the internal interaction mechanisms of the investigated alloys.

In the late 1990s [7] we analysed the average-pair distributions from EXAFS quaternary data in both $Cd_{1-x}Mn_xSe_yTe_{1-y}$ [4] and $Ga_xIn_{1-x}As_ySb_{1-y}$ [5]. In order to quantify ion SOPs, we developed an *ad hoc* semi-empirical model for these systems [7]. However, the strained tetrahedron model may be applied with success also to pseudo-quaternary materials such as these two systems. The estimations obtained by both methods are compared here.

The correlation between vibration spectra and the elemental tetrahedron structure of zincblende ternary systems was first analysed by Verleur and Barker [8,9]. For $GaAs_yP_{1-y}$ they considered the contributions of the *five* basic elemental tetrahedra to the vibration spectra. However, their one-parameter β model [8,9] is insufficient [10] to describe the configuration populations of FIR data of ternary systems in which SOPs are reported. As a consequence, to interpret FIR data we introduced an ad hoc model [11,12], derived from the strained tetrahedron model previously used to interpret EXAFS data [13-15]. In both models, a phonon mode observed in the reflectivity spectra [11,12] as an individual line from a lattice anion-cation pair can be associated with one of the possible *five* tetrahedron configurations, $\{T_k\}_{k=0,4}$ for ternary $A_{1-x}B_xZ$ or AY_yZ_{1-y} systems (see Fig.1 in ref. [13, 14]).

In $GaAs_yP_{1-y}$ [8] and $CdSe_yTe_{1-y}$ [9], the observed deviation from linearity of the experimental sum of oscillation strength vs. composition has been ascribed to a non-random distribution of anions within the lattice, i.e., a SOP distribution. This was the first well-documented information about SOPs from next nearest-neighbours (NNN) for ternary III-V and II-VI alloys. Additional EXAFS studies have been performed in CdHgTe [15], CdMnTe [16], CdZnTe [17], GaAlN [18], GaAsP [19], GaInAs [20], HgMnTe [15], HgZnTe [21], ZnMnS [22-

24], ZnMnSe [25,26] and ZnMnTe [27], while FIR spectra have been collected for CdHgTe[28], CdSeTe [29] and CdZnTe [30]. All these alloys clearly exhibit occupation preferences.

Using the strained tetrahedron model, in the first part of this paper, we analyse the EXAFS data of two sets of $Cd_{1-x}Mn_xSe_yTe_{1-y}$ [4] and one set of $Ga_{1-x}In_xAs_ySb_{1-y}$ [5]. SOP-coefficients were obtained via a quantitative evaluation of the respective constituent tetrahedron configurations through the values of *site occupation preference*. In the second part we present and discuss far IR CdMnSeTe phonon spectrum, using the preference W_k-coefficient values [1] obtained by analysis of the corresponding EXAFS data [4] .

While writing this contribution, experimental work performed by Romcevic *et al.* [31] based on FIR reflectivity and Raman spectra of $Cd_{1-x}Mn_xSe_yTe_{1-y}$ was published. These results were considered and are addressed in Section-6 of this paper.

2. Theoretical approach

Sphalerite canonical (i.e., without impurities, point defects and antisites) quaternary $A_{1-x}B_xY_yZ_{1-y}$ systems with 2-cations+2-anions can be viewed as composed of tetrahedron configurations ${}_cT^{i,j}_{k,4-k}$ with a *c*-ion at the centre, *c*= {A, B, Y, Z} and *k* and *4-k* ions at the vertexes, respectively (Y,Z) for *c*= A or B, and (B,A) for *c*= Y or Z. The constituent elemental configurations are thus *sixteen*: *four* binary configurations (with two ion species each) AZ, AY, BZ, BY and *twelve* ternary configurations (with three ion species each), $\{ {}_AT^{Y,Z}_{k,4-k}$, ${}_BT^{Y,Z}_{k,4-k}$, ${}_YT^{B,A}_{k,4-k}$, ${}_ZT^{B,A}_{k,4-k} \}_{k=1,3}$. To each of these we associated a SOP ${}_cW_k$ coefficient (relative to a random distribution), with $0 \le {}_cW_k \le 4/k$ for all three *k*'s and four *c*'s (see ref. [1]). The four binary configurations we arbitrarily label, AY as ${}_AT_4$ ($\equiv {}_AT^{Y,Z}_{4,0} \equiv {}_YT^{B,A}_{0,4} \equiv {}_YT_0$), BY as ${}_YT_4$ ($\equiv {}_YT^{B,A}_{4,0} \equiv {}_BT^{Y,Z}_{4,0} \equiv {}_BT_4$), AZ as ${}_ZT_0$ ($\equiv {}_ZT^{B,A}_{0,4} \equiv {}_AT^{Y,Z}_{0,4} \equiv {}_AT_0$), BZ as ${}_BT_0$ ($\equiv {}_ZT^{B,A}_{4,0} \equiv {}_BT^{Y,Z}_{0,4} \equiv {}_YT_4$), while $\{ {}_cW_0 = {}_cW_4 \}_{c=A,B,Y,Z} \equiv 1$ (see [1]). The respective ternary probabilities of ${}_cT_k$ in $A_{1-x}B_xY_yZ_{1-y}$ are

$$\{ \eta_c(x,y) \}_{c=A,B,Y,Z} = \{ ½(1-x),\ ½x,\ ½y,\ ½(1-y) \} \quad \text{respectively} \quad (\text{with } \Sigma_c\, \eta_c(x,y) \equiv 1). \qquad (1)$$

In a random distribution, the site filling (of *k* B ions in a shell with *N* sites [4 in the 1st shell, and 12 in the 2nd shell], from relative contents *x* and *1-x*) is precisely described by the Bernoulli binomials

$$\{ p_k[^{N]}(x) = N!/[k!(N-k)!]x^k(1-x)^{N-k} \}_{k=0,N} \qquad (2)$$

with $\Sigma_{k=0,N} \{ p_k[^{N]}(x) \} \equiv 1$ and $\Sigma_{k=0,N} \{ k\, p_k[^{N]}(x) \} \equiv Nx$.

Whenever the distribution is not random, the preference weight coefficients ${}_cW_k$ are applied to the Bernoulli binomials [1], and the corresponding ternary configuration probability is depressed with respect to the random case (${}_cW_k \equiv 1$), each time ${}_cW_k \neq 1$, by a factor

$$ {}_cC_k = \min[\, {}_cW_k,\ 1,\ (4-k\ {}_cW_k)/(4-k)] \le 1 \text{ (see [1])} \qquad (3)$$

This is due to the unbalanced quest of the ions in competition leading to a scarcity of one of the two contending ions with respect to the other. The ions in excess go to enhance the corresponding binary populations, AZ for ${}_ZW_k < 1$ and for ${}_AW_k < 1$, BZ for ${}_ZW_k > 1$ and ${}_BW_k < 1$, AY for ${}_YW_k < 1$ and ${}_AW_k > 1$, BY for ${}_BW_k > 1$ and ${}_YW_k > 1$. This fully defines for $A_{1-x}B_xY_yZ_{1-y}$ the probabilities $\{ {}_cP_k(x,y) \}_{c=A,B,Y,Z;\ k=0,4}$ for all twelve ternary configurations $\{ {}_cT_k \}_{c=A,B,Y,Z;\ k=1,3}$, with

the variable ${}_c\nu(x,y)$ in the Bernoulli binomial defined for c=Y or c=Z as ${}_c\nu(x,y)=x$, while for c=A or c=B, it is ${}_c\nu(x,y)=y$.

$$\{ {}_cP_k\ (x,y) = \eta_c(x,y)\ {}_cC_k\ p_k^{[4]}[\ {}_c\nu(x,y)] \}_{k=1,3} \qquad \text{for ternary } T_k$$

with $\{ {}_cC_k\ (W_k)\}_{k=1,3}$, corrective weight factors imposed by the stoichiometry of x or y

$$0 \le \{ {}_cC_k = \min[W_k, 1, (4-kW_k)/(4-k)] \}_{k=1,3} \le 1$$

$W_k<1$ enhances binary AZ populations, while $W_k>1$ that of binary BZ, i.e.,

$$ {}_cP_0\ (x,y) = \eta_c(x,y)\ \{\ p_0^{[4]}(x) + \Sigma_{k=1,3}\ [\ \max(0,\ 1-W_k)\ p_k^{[4]}\ (x)\ ]\ \} \qquad \text{for binary } AZ \text{ configuration } T_0$$

$$ {}_cP_4\ (x,y) = \eta_c(x,y)\ \{\ p_4^{[4]}(x) + \Sigma_{k=1,3}[\ \max(0,\ k(W_k-1)/(4-k))\ p_k(x)\ ]\ \} \qquad \text{for binary } BZ \text{ configuration } T_4$$

(4)

In the random case, when $\{W_k \equiv 1\}_{k=1,3}$, $\{ {}_cP_k^{[4]}(x,y) \rightarrow \eta_c(x,y)\ p_k[\ {}_c\nu(x,y)] \}_{k=0,4}$.

Following the evolution of SOP values of a pure ternary ($\text{ternary}_{(\text{as T})}$) as it is being *diluted* in a pseudo-quaternary system ($\text{ternary}_{(\text{in Q})}$) gives information on the system thermodynamics.

The above considerations are valid for zincblende structures, but can also be extended to the tetrahedron coordinated wurzite (hexagonal) structures when the predominant contribution to physical properties comes from NN and NNN atomic neighbours. Thus the approach can be applied to analysis of $A_{1-x}B_xY_yZ_{1-y}$ EXAFS data of both zincblende and wurzite structures.

3. EXAFS data analysis of $<{}_i^jCN>$ (x)> and $<{}_i^jd>$ (x)>

EXAFS (see theoretical considerations in ref.s [32,33]) is one of the most widespread investigation methods used to characterise the local structures of an ordered system. EXAFS analysis is usually performed by selecting the x-ray energy at the K-edge value of the atom under investigation or, with some limitations, for high-Z elements at the energy of the L-edge value. The standard EXAFS equation, formulated in the generally accepted short-range single-electron theory [34] expressed in the k-vector space, is

$$\Pi(k) = 1/k\ \Sigma\ A_j(k)\ \sin[N_j(k)]$$

where $N_j(k)$ is the total phase of electron scattering in the k-vector space, with subscript j summed over all coordinate shells, while $A_j(k)$, the EXAFS amplitude, is given by

$$A_j(k) = N_j/R_j^2\ |f_j(B,k)|\ \exp(-2R_j/\delta)\ \exp(-2\Phi_j^2k^2)\ , \qquad (5)$$

where $f_j(B,k)$ is the back scattering amplitude from each of the N_j neighbouring atoms of the j^{th} type situated at position R_j , and Φ_j is the Debye-Waller factor that accounts for thermal vibrations of the atomic bonding. Finally, the term $\exp(-2R_j/\delta)$ accounts for inelastic losses in the scattering process, with δ the attenuation factor.

The formula bears information on the neighbouring ions of the photoexcited ion. Apart from the complexity of the expression, it is easily seen that the amplitude of the signal is proportional to the number of neighbours in the successive shells. Due to the large tuning of the electron wavelength because of scattering losses, the materials are commonly studied through relations between the c-atom and its nearest-neighbours (NN) and next nearest-neighbours (NNN), and only in selected cases for next next nearest-neighbours (NNNN).

For the quaternary four constituent ions c={A, B, Y, Z} of the sample under investigation (of relative content x), this reveals the <u>average</u> (over the sample and over all configurations)

local structure around this *c*-ion, of ***1***) the relative number of ions of a given type around it, i.e., ion pairs or coordination numbers (CN), $<{}^{j}_{c}CN\ (x)>$; ***2***) inter-ion distance $<{}^{j}_{c}d\ (x)>$ between the selected *c*-ion and the NN or NNN *j*-ions around it. We prefer to use the mnemonic symbolism to the traditional R_i and N_i currently used in EXAFS analysis and cited in the previous paragraph.

The probability ${}_{c}P_{k}\,(x,y)$ of an NN ion-pair ij= {AY, AZ, BY, BZ} is the product of the corresponding ${}_{c}\eta$ times the configuration probability (Eqs. 1 and 3). As an example, for a *substituting* ion at the vertex, we have,

for ZB from ${}_{Z}T$: ${}_{Z}\eta(y)$ k ${}_{Z}W_{k}$ $p_k^{[4]}(x)$

while for an ion *being substituted*:

for AZ from ${}_{A}T$: ${}_{A}\eta(x)$ (4-k ${}_{A}W_{k}$) $p_k^{[4]}(y)$, or

(the full set of equations is given in Table-A1 of the appendix).

The NN average coordination numbers $<{}^{j}_{i}CN\ (x)>$ is a *count* of pair numbers and, though configuration independent, EXAFS may discriminate (due to the K-edge selectivity) an ij-pair depending on whether it comes from the configuration ${}_{i}T$ or ${}_{i}T$. Because they are not correlated to each other, we have to distinguish between ${}^{j}_{i}CN$ and ${}^{i}_{j}CN$. From the expressions for the ternary such as $<^{AZ}CN>$, $<^{BZ}CN>$, $<^{AZ}d>$, $<^{BZ}d>$ taken from [1], one can write for each ${}^{NN\ dipole}<CN(x,y)>$ of the pseudo-quaternary $A_{1-x}B_xY_yZ_{1-y}$ four pairs of equations. For an ion *being substituted* we have:

$$<{}^{Z}_{A}CN\ (y)> = \Sigma_{k=0,3}[(4-k\ {}_{A}W_{k})p_k^{[4]}(y)] = 4 - <{}^{Y}_{A}CN\ (y)>$$

(the full set of equations is reported in Table-A2 of the appendix). A similar set of equations is obtained for the average NN inter-ion distances $<^{ij}d>$ [1]. These depend on the configuration they belong to; hence the stoichiometry has to be accounted for using the ${}_{c}C_{k}$ coefficients (Eq.1) instead of the ${}_{c}W_{k}$ coefficients. Whence, as for the ${}^{v}_{c}CN$'s, one has for the ${}^{v}_{c}d$'s, for an ion *being substituted*:

$$<{}^{Z}_{A}d\ (x,y)> =$$
$$\{(1-x)\ \Sigma_{k=0,3}\{{}^{Z}_{A}d_k\,(4-k\ {}_{A}C_{k}) + 4\,{}^{AZ}_{A}d_0\ \max(0,1-{}_{A}W_{k}) + 4\,{}^{AZ}_{A}d_4\ \max[0,(k\ {}_{A}W_{k}-1)/(4-k)\}\ p_k^{[4]}(y)\}$$
$$/\ \{\ (1-x)\ \Sigma_{k=0,3}\{(4-k\ {}_{A}C_{k}) + 4\ \max(0,1-{}_{A}W_{k}) + 4\ \max[0,\ (k\ {}_{A}W_{k}-1)/(4-k)]\}\ p_k^{[4]}(y)\ \}$$

(the full set of equations is reported in the Table-A3 of the Appendix)

4. Quaternary EXAFS data interpretation

As mentioned in the introduction, a rough three-parameter semi-empiric approximation was applied to fit the reported coordination number $<{}^{j}_{c}CN\ (x)>$ preferences [7] of two sets of EXAFS data of the $A_{1-x}B_xY_yZ_{1-y}$ type quaternary systems, namely $Ga_xIn_{1-x}As_ySb_{1-y}$ [5] and $Cd_{1-x}Mn_xSe_yTe_{1-y}$ [4]. The GaInAsSb structure remains mono-phase zincblende structured at all compositions, i.e., x∈[0;1] and y∈[0;1], while CdMnTeSe does so when simultaneously x<0.2 and y<0.2. We recall that in this model we attribute *weight coefficient* factors w_k to the Bernoulli (random distribution) binomials. The result, for GaInAsSb, gave $\{w_k\}_{k=1,3}$={2.19, 1.07, 1.64} (see Table-1) and, for CdMnTeSe, $\{w_k\}_{k=1,3}$={1.9, 1.6, 1.3}, see Table-2. (We recall

here that for a random site occupation without preferences $\{w_k\}_{k=1,3}\equiv 1$.) The semi-empiric approximation returns an excellent fit to the experimental results for both quaternary systems [7]. However, following the introduction of the strained tetrahedron model [1] it was established that the elemental tetrahedron distribution (with four NN sites to be filled) in the sphalerite and in the wurzite crystal structures (limited to the first two shells, NN and NNN) have coefficients

1) expressly bound by two *extreme values* $\{0\le w_k\le 4/k\}$,

2) and departure from the random distribution leading to an automatic decrease in the corresponding tetrahedron population (see ref. [1]).

Thus, the semi-empiric approximation gives a value of $w_3=1.64$ for GaInAsSb, which is beyond the allowed range ($w_3\le 4/3$), in violation of the physical condition of coordination conservation. However, in both materials the T_3 configuration is evanescent (see Table-2) because, when one of the competing ions through an extreme preference *grabs* all four available tetrahedron sites, the other ion type has no sites available to form a ternary, and only binary systems are possible. We have to underline that while the coefficients w_k used in the semi-empirical treatment are just numerical parameters, in the strained tetrahedron model, W_k are physical values related to the number of available occupation sites. We will now reinterpret the data of these alloys (see ref. [13]) in the framework of the *strained-tetrahedron* model [1,13,14] to evaluate the improvement with respect to previous estimations.

4.1. $Ga_xIn_{1-x}As_ySb_{1-y}$ analysis

Islam and Bunker [5] investigated the quaternary $Ga_xIn_{1-x}As_ySb_{1-y}$ which crystallises in the tetrahedron coordinated zincblende monophase structure for all *x* and *y* compositions. They reported an EXAFS investigation at the As K-edge for eight different compositions: five with $y_{As}=0.05$, $x_{Ga}=\{0.2, 0.5, 0.65, 0.8, 0.95\}$ and three with $y_{As}=0.10$, $x_{Ga}=\{0.1, 0.5, 0.9\}$. Applying the strained tetrahedron model to this set of data, one may obtain both preferences and inter-ion distances for a ternary $GaInAs_{(in\ Q)}$ in a quaternary medium (see Table-1).

Previously, Mikkelson and Boyce [20] studied, using the As K-edge, ternary $Ga_{1-x}In_xAs$ as a pure ternary ${}_{As}T^{In,Ga}_{k,4-k}$ system. The deconvolution of his results returns SOP values $\{W_1= 1.05, W_2= 0.25, W_3= 0.58\}$, see ref. [1]. The $GaInAs_{(as\ T)}$ ${}^{Ga}_{As}d_k$ and ${}^{In}_{As}d_k$ values are also reported in Table-1 [1].

Comparing the values of the $GaInAs_{(as\ T)}$ with those of the $GaInAs_{(in\ Q)}$ obtained by the deconvolution of a quaternary [5] we recognised the evolution of the preferences of this ternary as a component of a quaternary system. Moreover, we have to underline here also that Islam's data refer to a quaternary medium heavily *Sb*-loaded ($y_{Sb}=(1-y_{As})\ge 0.90$, since $y_{As}\le 0.10$). For the sake of clarity, the model-derived ${}^{Ga}_{As}d_k$ and ${}^{In}_{As}d_k$ inter-ion distances of the $GaInAs_{(in\ Q)}$ are reported with those obtained for $GaInAs_{(as\ T)}$ [1]. Comparison of Islam and Bunker [5] experimental NNN average coordination number values and their two best fit curves (as a function of "*x*") are given in Fig.1. Fit was performed using both

a) the semi-empirical approach (dashed curve) and

b) the strained-tetrahedron model (full curve).

The approaches show good agreement with experimental data, but in Fig.1 while curve ***b*** remains throughout with CN≤4, curve ***a*** violates the CN extreme condition, exceeding the limit

of CN=4. The slight deviation of the results for y_{As}=0.10 from those of the five for y_{As}=0.05 is to be attributed to the fact that the y=0.10-set is a *fit* based on only three points and three parameters (W_1, W_2, W_3), while the y=0.05-set is based on five points and is a true *best fit*, free of the rigidity that is liable to reproduce local point value uncertainties. Thus, we can claim that in the range <0.05 – 0.10> SOP coefficients are stationary and are those labelled as *both together*. These values are quite different from those of the y_{As}=1 values of the pure ternary obtained by Mikkelson and Boyce (see bottom row). The discrepancy is addressed in the discussion section.

4.2 $Cd_{1-x}Mn_xSe_yTe_{1-y}$ analysis

The Q22 system $Cd_{1-x}Mn_xSe_yTe_{1-y}$ has a complex phase transition diagram [35]; when simultaneously both x<0.2 and y<0.2, the structure is mono phase zincblende. Kisiel et al. [4] investigated four samples: three $Cd_{1-x}Mn_xSe_{0.1}Te_{0.9}$ with x_{Mn}={0.05, 0.10, 0.15), and one $Cd_{0.8}Mn_{0.2}Se_{0.2}Te_{0.8}$, and reported EXAFS results for nearest-neighbours [4] both of <CN> coordination numbers and of <d> distances. Analysis of quaternary NN $Cd_{1-x}Mn_xSe_yTe_{1-y}$ data (at the K-edges of both Mn and of Se) yields information on both ${}_{Mn}T_{k,4-k}^{Se,Te}$ and ${}_{Se}T_{k,4-k}^{Mn,Se}$ configurations. The peculiarity of the EXAFS analysis is that the method selects, at the Mn K-edge and Se K-edge, the **Mn**$Se_yTe_{1-y\ (in\ Q)}$ or $Cd_{1-x}Mn_x$**Se** $_{(in\ Q)}$ components in the quaternary environment respectively. Applying the strained tetrahedron model [1,13] to the reported data (24 experimental values), we obtain the following SOP C_k-coefficient values: **a)** $Cd_{1-x}Mn_xSe$ *(in Q)*, {C_k}={0.54,0,0}; **b)** $Cd_{1-x}Mn_xTe$ *(in Q)* , {C_k}={0.26,0,0}; while those of a pure ternary $CdMnTe_{(as\ \ T)}$ [16] are {C_k}={0.68, 0.67,0}; **c)** $CdSe_yTe_{1-y}$ *(in Q)*, {C_k}={0.54,0,0}; **d)** $MnSe_yTe_{1-y}$ *(in Q,* {C_k}={0.26,0,0.20} (Tab.2). The corresponding coordination number curves are given in Fig.2.

5. Analysis of $Cd_{1-x}Mn_xSe_yTe_{1-y}$ phonon spectra

To check the hypotheses that a pseudo-quaternary system like $Cd_{1-x}Mn_xSe_yTe_{1-y}$ behaves as a *linear* combination of the contributions of its related four ternary components, we measured the FIR spectra, i.e., the phonon spectra of each of the ternary constituent systems. The $Cd_{1-x}Mn_xSe_yTe_{1-y}$ samples are those previously investigated by EXAFS [4].

Actually, a pseudo-quaternary can be viewed as a combination of ternaries, so its phonon spectrum should exhibit *ternary* behaviour as described in ref.s [11,12]. Similarly to the FIR spectrum of a ternary, the expression for the dielectric function of an $A_{1-x}B_xY_yZ_{1-y}$ quaternary system is

$$\varepsilon(\omega, x, y) = \varepsilon_\infty + \Sigma_{j=1,n}\{S_j\omega^2_j/[(\omega^2-\omega^2_j)+i\,\omega\Gamma_j] = \varepsilon_1(\omega, x, y) + i\,\varepsilon_2(\omega, x, y) \qquad (6)$$

where {ω_j, Γ_j, and S_j} are, respectively, the frequency, the line half-width and the oscillator strength of the Lorentzian line components of the spectrum. The FIR phonon spectrum of an $A_{1-x}B_xZ$ ternary can be written as the superposition of the contributions of its iZ-dipoles (i=A or i=B) from the respective five configurations: one phonon from each of the two binary configurations ${}_ZT_{0B}$ and ${}_ZT_{4B}$, and a phonon from each of the AZ and BZ dipoles from each of the three ternary configurations ${}_ZT_{1B}$, ${}_ZT_{2B}$, ${}_ZT_{3B}$, i.e., a total of eight phonons in two mode-bands. The oscillator strength of each phonon is determined by the configuration probabilities $P_k(x)$'s

defined by Eq.(4), which takes into account the preferences and the specific oscillator strengths of the two AZ and BZ binary systems. The expression for $\varepsilon_2(\omega,x)$ is given in the appendix (Eq.6).

5.1 Experimental investigation of FIR reflectivity

The quaternary CdMnSeTe crystals, previously investigated by EXAFS [4], were investigated here by means of IR reflectivity, i.e., one $Cd_{0.8}Mn_{0.2}Se_{0.2}Te_{0.8}$ and two $Cd_{1-x}Mn_xSe_{0.1}Te_{0.9}$ with x_{Mn}={0.05, 0.15). The crystals were grown by the Bridgman method [36] in mono-phase zincblende crystals (all crystals fulfil simultaneously x≤0.2 and y≤0.2) [35]. For these experiments, the crystal samples were cut in sizes ≈ 0.5 × 0.5 × 0.2 cm^3, and their surfaces prepared for the optical measurements.

The IR reflectivity measurements were performed at the DAΦNE-light laboratory at Frascati [37] using a BRUKER Equinox 55 FT-IR interferometer modified to collect spectra under vacuum, a liquid helium bolometer of IRLABS and a Hg-lamp as light source. During the experiments the vacuum pressure was kept at $<10^{-3}$ mbar. A JANIS helium-cooled cryostat was used for measurements at low temperature in the range 10-300 K. The reflectivity was measured using a gold film evaporated onto the surface of the investigated samples as reference. This method enabled us to measure the reflectivity coefficient with an accuracy of about 1%. The spectral resolution was 2 cm^{-1} and we usually collected 200 scans for each T within <1000 s of acquisition time.

The FIR reflectivity phonon spectrum of each single crystal was observed in the 20-700 cm^{-1} frequency range, both at room temperature and at a low temperature, between 10 and 30 K. All reflectivity spectra are shown in Fig.3A. From each spectrum, using the Kramers-Kronig transformations, and being careful of the finite experimental ω-range, we obtained the corresponding real (ε_1) and imaginary (ε_2) parts of the dielectric constant ε (Eq.6). ε_2 spectra are shown in Fig.3B where the maxima of each oscillator line are directly visible in each spectrum. We assumed either Gaussian or Lorentzian lines, both characterised by the three parameters {ω_j, Γ_j, and A_j}. The Microsoft Office Excel 2003 Solver program was used to fit the analysed functions, by minimising the sum of quadratic deviations.

As is evident in Fig.3B the CdTe-dipole-related mode band at about 140-144 cm^{-1} is the dominant one, but at least three bands related to lighter dipole pairs, namely CdSe, MnTe and MnSe, can be detected at about 170-185 , 185-190 and 205-210 cm^{-1}, respectively (see Fig.3B.a). Frequencies are affected by a red shift of up to 6 cm^{-1} as the temperature is increased from low to room.

5.2 FIR spectrum analysis

The ε_2 Kramers-Kronig transformations of the observed reflectivity phonon spectra are the envelops of the phonon lines. According to our hypothesis each line is linked to an anion-cation dipole from each of the five tetrahedron configurations of the four ternary components of the quaternary system. Each ternary configuration contains two bands, each correlated to one of the two different dipole types vibrating in the ternary tetrahedron, leading to potentially four phonon lines. The expression of the overall oscillator strength of a ternary spectrum is given in (Eq.6) [11,12] and is the sum of the contributions of each of its eight phonon lines, linked to one of the

two kinds of its cation-anion dipole oscillators. Besides its frequency, each oscillator is characterised by two parameters, the half-width and the specific oscillator strength. The line amplitude is the product of several factors, such as the dipole specific binary oscillator strength, the dipole multiplicity of that configuration, and the probability P_k of the configuration (see Eq.4). Because the oscillator strength of a pseudo-quaternary is the sum of the four spectra of the ternary components, 32 lines are expected. Each line belongs to a phonon mode-band of a given cation-anion dipole.

The *ab initio* analysis consisted in attempting to fit all measured FIR spectra, with 32 plus 4 lines (to take into account additional vibrations such as those of point defects or impurities), each one defined by its three parameters (ω_i, Γ_i, A_i) and with the only constraint that the set $\{\omega_i\}_{i=1,36}$ be a monotonous increasing set, with $\omega_i - \omega_{i-1} > 2$ cm^{-1} (to account for the experimental resolution). With such a large number of parameters, the fits return a good agreement with experimental data (an illustration is given in Fig.4a). Important to note is that the fits return nil amplitudes for several lines, i.e., the corresponding phonon modes are not detected. Indeed, this fitting method does not allow a reliable identification of the lines. As a consequence we reconsider the analysis of the zincblende $A_{1-x}B_xY_yZ_{1-y}$ systems with our model.

6. Discussion

To verify the hypothesis that a pseudo-quaternary $A_{1-x}B_xY_yZ_{1-y}$ system is really composed of only binary and ternary tetrahedron configurations, we try to fit the spectra using the preference C_k-coefficients as derived in the CdMnTeSe compound by EXAFS analysis [4] (Eqs. 3-5, and Table 2). Within this model each line is correlated to a dipole mode of a given configuration and the intensities explicitly reflect the respective ion contents, the configuration probabilities including preferences, the configuration multiplicity and the dipole oscillator strength. For the 32 lines previously defined, the frequencies are set to respect the frequency hierarchy within each mode band (ordered inversely to the configuration mass). The frequency sequences of the two parallel hierarchy relations are given in Table A4 of the appendix. Again to fulfil the experimental resolution, we impose within each sequence that $(\omega_i - \omega_{i-1}) \geq 2$ cm^{-1}.

Seven tetrahedron configurations $\{ {}_{Mn}T_{2,2}^{Se,Te}, {}_{Se}T_{2,2}^{Mn,Cd}, {}_{Se}T_{3,1}^{Mn,Cd}, {}_{Cd}T_{2,2}^{Se,Te}\ {}_{Cd}T_{3,1}^{Se,Te}, {}_{Te}T_{2,2}^{Mn,Cd}, {}_{Te}T_{3,1}^{Mn,Cd} \}$ turn out to be negligible due to the extreme preferences observed, as quantified by the C_k values derived from EXAFS data analysis. This means that fourteen frequencies have to be neglected (see the 14 shaded-grey frequencies in Table A4 of the appendix). Hence we expect that:

1) the intensities of the four ${}^{CdTe}\omega$, ${}^{MnTe}\omega$, ${}^{CdSe}\omega$, ${}^{MnSe}\omega$ lines from the *binary* configurations will be enhanced with respect to their random values;
2) only eight lines: ${}_{Cd:1Se}\omega_{1,3}^{Se,Te}$, ${}_{Cd:3Te}\omega_{1,3}^{Se,Te}$, ${}_{Se:1Mn}\omega_{1,3}^{Mn,Cd}$, ${}_{Se:3Cd}\omega_{1,3}^{Mn,Cd}$, ${}_{Te:3Cd}\omega_{1,3}^{Mn,Cd}$, ${}_{Te:1Mn}\omega_{1,3}^{Mn,Cd}$, ${}_{Mn:1Se}\omega_{1,3}^{Se,Te}$, ${}_{Mn:3Te}\omega_{1,3}^{Se,Te}$ will be detectable,
3) Due to the low values of relative contents $x \leq 0.15$ and $y \leq 0.2$, the two lines ${}_{Mn:3Se}\omega_{3,1}^{Se,Te}$ and ${}_{Mn:1Te}\omega_{3,1}^{Se,Te}$ should have low intensities, which are hard to detect.

Then, we proceed to check the presence of extreme preferences in the pseudo-quaternary CdMnTeSe. For a quaternary $A_{1-x}B_xY_yZ_{1-y}$ tetrahedron configuration with an "*i*" centred ion and "*m*" "*j*" vertex ions, we write ${}_i^j\Gamma_m$ for the half width and ${}_i^jA_m$ for the amplitude. In agreement with refs. [11,12] we consider $\{{}_i^j\Gamma_m\}_{m=1,4} = {}_i^j\Gamma$, and $\{{}_i^jA_m\}_{m=1,4} = {}_i^jA$. Finally we consider the *eight*

parameters ${}_{A}{}^{Y}\Gamma$, ${}_{A}{}^{Z}\Gamma$, ${}_{B}{}^{Y}\Gamma$, ${}_{B}{}^{Z}\Gamma$, ${}_{Y}{}^{A}\Gamma$, ${}_{Y}{}^{B}\Gamma$, ${}_{Z}{}^{A}\Gamma$, ${}_{Z}{}^{B}\Gamma$ and the *eight* parameters ${}_{A}{}^{Y}A$, ${}_{A}{}^{Z}A$, ${}_{B}{}^{Y}A$, ${}_{B}{}^{Z}A$, ${}_{Y}{}^{A}A$,□ ${}_{Y}{}^{B}A$, ${}_{Z}{}^{A}A$, ${}_{Z}{}^{B}A$, e.g., one parameter-pair per a given mode-band ion-pair dipole. We refer to such an approximation as the *8+8* approximation, with the corresponding deconvolution illustrated in Fig.4b.

In a quaternary system, an *ij*-ion-pair dipole occurs in two distinct ternaries. We thus investigate an even more stringent approximation in which we consider that ${}_{i}{}^{j}\Gamma = {}_{j}{}^{i}\Gamma = {}^{ij}\Gamma$, i.e., 4 parameters ${}^{AY}\Gamma$, ${}^{AZ}\Gamma$, ${}^{BY}\Gamma$, ${}^{BZ}\Gamma$, and ${}_{i}{}^{j}A = {}_{j}{}^{i}A = {}^{ij}A$, i.e., another 4 parameters ${}^{AY}A$, ${}^{AZ}A$, ${}^{BY}A$, ${}^{BZ}A$ so that the model becomes a *4+4* approximation, with the corresponding deconvolution illustrated in Fig.4c. Comparing Figs.4b and 4c, both approximations are in good agreement with spectral shapes. The respective *normalised sum-quadratic-deviation* "variances (σ^2)" show that both the *8+8* and the *4+4* approximations are consistent and indeed equivalent because for the spectral signal in the ω-range [100-240] cm^{-1} the relative σ^2 is between <0.5-2.8>% for the *4+4* approximations, while it is confined between <0.4-1.4>% for the *8+8* approximations (see Table-3). The result confirms that in a quaternary system, to a first approximation, and as has been shown in ternary systems, the line shape and the specific oscillator strength are characteristic of the ion pair of the emitting dipole and are independent of the multiplicity of the emitting configuration. Moreover, it appears that in pseudo-quaternary systems, the phonon oscillator strength from an AZ-dipole remains invariant, independently of the corresponding configuration of the ternary system $A_{1-x}B_xZ$, i.e., with A at the tetrahedron centre and Z at a vertex, or as in AY_yZ_{1-y} i.e., with Z at the tetrahedron centre and A at a vertex. In other words it is independent of the respective centre-vertex positions of the ions within the tetrahedron.

Romcevic *et al.* [31] observes in the far-infrared $Cd_{1-x}Mn_xSe_yTe_{1-y}$ spectra three TO-modes at about 140 cm^{-1} (CdTe), 170 cm^{-1} (CdSe related) and 205 cm^{-1} (MnTe related), while in the Raman spectra only the first two modes. In our FIR spectra, we do identify three bands, but assign them to four overlapped modes, extending between the two extreme ${}^{CdTe}\omega_{<139.5\text{-}145.6>}$ and ${}^{MnSe}\omega_{<205\text{-}220>}$ frequency modes, with the intermediate $\mathbf{{}^{CdSe}\omega_{<165\text{-}173.5>}}$ mode and the additional $\mathbf{{}^{MnTe}\omega_{<185.7\text{-}191.2>}}$ frequency. The existence of such bands, with their oscillator strengths weighted by their probabilities (<72-85.5>% for CdTe, <8.5-18>% for CdSe, <4.5-13.5>% for MnTe and <0.5-2>% MnSe), may support a line overlap with a consequent overall envelop clearly detected in our data (see Fig.3B.a).

7. Conclusion

Three of the four CdMnSeTe samples investigated by EXAFS measurements have been investigated with FIR reflectivity. The main results addressed by the analysis presented in this paper are:

- The strained tetrahedron model, originally applied to ternary tetrahedron coordinated systems, can be applied with success also to interpret pseudo quaternary systems of type $A_{1-x}B_xY_yZ_{1-y}$.
- Comparison between the semi-empirical approach and the strained tetrahedron models applied to the analysis of pseudo-quaternary shows that both are reliable models and their best fit curves reproduce the EXAFS experimental data at room temperature within the experimental error bars.

- Systems with a pseudo-quaternary zincblende structure can be described by a superposition of binary and ternary elemental tetrahedrons.

The strained tetrahedron model has also been applied to analyse and interpret the FIR phonon spectra of quaternary $Cd_{1-x}Mn_xSe_yTe_{1-y}$.

- To a first approximation, both line shapes and intensities in pseudo-quaternary and in ternary systems are determined by the cation-anion dipole pair, and are unaffected by the centre-vertex position of the dipole within the tetrahedron configuration. Indeed, observing the best-fit results (Table-3) of approximations 8+8 vs. 4+4, on the one hand, as expected, confirms the better convergence with 8+8 compared to that with fewer parameters 4+4, while on the other hand the closeness of the returned s^2_{8+8} and s^2_{4+4} , s^2 values speaks in favour of our assumption that the two phonons emitted by a dipole ${}^{A}_{Z}$ from the ternary $A_xB_{1-x}Z$ and by ${}_{A}^{Z}$ from the complementary AY_yZ_{1-y}, are with a good approximation equal.
- Since FIR spectra show a trend vs. temperature of the molecular vibrations, an EXAFS analysis vs. T could be interesting, in particular for the analysis of the Debye-Waller parameters in these materials.
- EXAFS analysis and FIR phonon spectra of pseudo-quaternary systems indicated that they can be described by a linear superposition of the contributions of the four ternary components, and the strained tetrahedron model, originally designed to model ternary systems, can also be applied with success to these compounds. Preferences in quaternary systems are quantified by coefficients; when the relative contents change, so do preference values (see preference coefficients for $Ga_xIn_{1-x}As_{(as\ T)}$ in which the second shell ions around an As-anion are all As-anions, while those in $Ga_xIn_{1-x}As_{0.05}Sb_{0.95}$ of $Ga_xIn_{1-x}As_{(in\ Q)}$ in which the second shell ions around an As-anion are almost all Sb-anions).
- The evolution of the SOP-coefficients, as a ternary is *progressively diluted* within the pseudo-quaternary, may be considered as a valuable index of the thermodynamic evolution of the system. Indeed, the heterogeneous presence of competing ions in the NNN shell profoundly modifies the SOPs with respect to the corresponding pure ternary (which has a perfectly homogeneous NNN shell composition).
- A true-quaternary system is characterised by three ions competing for site occupation in a shell bounded on both sides by shells of the complementary sublattice with homogeneous mono-ions! The pseudo-quaternary system is conditioned by site occupation competition in both the cation and the anion sublattices, i.e., all shells. Whence, in a pseudo-quaternary system Q22 preferences are conditioned by relative concentrations; in a true-quaternary system, Q31 and Q13 are not.

Several investigations have shown that most semiconductors exhibit SOPs. Through analysis of these data, quantitative preference coefficient values can be reliably obtained using different models. Among them, the strained tetrahedron model has been applied with good agreement to both EXAFS data [1,13] and FIR spectra [11,12] of sphalerite ternary $A_{1-x}B_xZ$ and AY_yZ_{1-y}, and now to pseudo-quaternary $A_{1-x}B_xY_yZ_{1-y}$ (2-cation +2-anion) systems. With some limitations, it turns out to be successful also in the interpretation of wurzite [13] and intermetallic $M_3(XX')$ [14] systems, returning a quantitative evaluation of the SOPs.

In many semiconductors, SOPs return *extreme* values. Such behaviour indicates that a *ternary* filling of one (sometimes two of the three) elemental configuration does not occur. This

seems to be related to the thermodynamic creation affinity of cation-anion pair components in ternary or quaternary systems. A wide group of semiconductors presents such *missing* configurations. Understanding the phenomenon responsible for such behaviour would lead to a deeper knowledge of semiconductor behaviour.

Appendix

The far infrared phonon spectrum of an $A_{1-x}B_xZ$ ternary

$$\begin{aligned}\varepsilon_2(\omega,x) = \{ & \{4\ {}^{AZ}s_0\ {}^{AZ}\omega_0{}^2\ {}^{AZ}\Gamma_0\ \omega / [(\omega^2 - {}^{AZ}\omega_0{}^2)^2 + {}^{AZ}\Gamma_0{}^2\ \omega^2]\}\ P_0(x) && \textit{binary AZ}\\ & + \Sigma_{k=1,3}\ \{k\ {}^{BZ}s_k\ {}^{BZ}\omega_k{}^2\ {}^{BZ}\Gamma_k\ \omega / [(\omega^2 - {}^{BZ}\omega_k{}^2)^2 + {}^{BZ}\Gamma_k{}^2\ \omega^2] && \\ & + (4-k)\ {}^{AZ}s_k\ {}^{AZ}\omega_k{}^2\ {}^{AZ}\Gamma_k\ \omega / [(\omega^2 - {}^{AZ}\omega_k{}^2)^2 + {}^{AZ}\Gamma_k{}^2\ \omega^2]\} P_k(x) && \textit{ternary ABZ}\\ & + \{4\ {}^{BZ}s_4\ {}^{BZ}\omega_4{}^2\ {}^{BZ}\Gamma_4\ \omega / [(\omega^2 - {}^{BZ}\omega_4{}^2)^2 + {}^{BZ}\Gamma_4{}^2\ \omega^2]\}\ P_4(x)\ \} && \textit{binary BZ} \qquad (6)\end{aligned}$$

with the $P_k(x)$'s defined by Eq.(5)

Tab.A1 The eight equations defining the probabilities ${}_cP_k$ (x,y) of an NN ion-pair ij= {AY, BZ} (i.e., the product of the corresponding η times the configuration probability (Eqs. 1 and 3))

AZ from ${}_AT$: $\eta_A\ (4-k\ {}_AW_k)\ p_k^{[4]}(y)$	ZA from ${}_ZT$: $\eta_Z\ (4-k\ {}_ZW_k)\ p_k^{[4]}(x)$
BZ from ${}_BT$: $\eta_B\ (4-k\ {}_BW_k)\ p_k^{[4]}(y)$	ZB from ${}_ZT$: $\eta_Z\ k\ {}_ZW_k\ p_k^{[4]}(x)$
AY from ${}_AT$: $\eta_A\ k\ {}_AW_k\ p_k^{[4]}(y)$	YA from ${}_YT$: $\eta_Y\ (4-k\ {}_YW_k)\ p_k^{[4]}(x)$
BY from ${}_BT$: $\eta_B\ k\ {}_BW_k\ p_k^{[4]}(y)$	YB from ${}_YT$: $\eta_Y\ k\ {}_YW_k\ p_k^{[4]}(x)$

Tab.A2 The eight equations defining the average NN coordination numbers $<{}_i^jCN$ (x)>, (to distinguish between ${}_i^jCN$ and ${}_j^iCN$) for each NN ij-dipole of a pseudo-quaternary $A_{1\square x}B_xY_yZ_{1-y}$; pre-subscript *c*-centre ion, pre-superscript *v*-vertex ion

NN dipole <CN(x,y)>	Quaternary $A_{1-x}B_xY_yZ_{1-y}$
AZ $<{}_A^ZCN$ (y)>=	$\Sigma_{k=0,3}[(4-k\ {}_AW_k)p_k^{[4]}(y)] = 4 - <{}_A^YCN$ (y)>
$<{}_Z^ACN$ (x)>=	$\Sigma_{k=0,3}[(4-k\ {}_ZW_k)p_k^{[4]}(x)] = 4 - <{}_Z^BCN$ (x)>
BZ $<{}_B^ZCN$ (y)>=	$\Sigma_{k=0,3}[\ (4-k\ {}_BW_k)p_k^{[4]}(y)] = 4 - <{}_B^YCN$ (y)>
$<{}_Z^BCN$ (x)>=	$\Sigma_{k=1,4}[\ k\ {}_ZW_k\ p_k^{[4]}(x)] = 4 - <{}_Z^ACN$ (x)>
AY $<{}_A^YCN$ (y)>=	$\Sigma_{k=1,4}[\ k\ {}_AW_k\ p_k^{[4]}(y)] = 4 - <{}_A^ZCN$ (y)>
$<{}_Y^ACN$ (x)>=	$\Sigma_{k=0,3}[\ (4-k\ {}_YW_k)\ p_k^{[4]}(x)] = 4 - <{}_Y^BCN$ (x)>
BY $<{}_B^YCN$ (y)>=	$\Sigma_{k=1,4}[\ k\ {}_BW_k\ p_k^{[4]}(y)] = 4 - <{}_B^ZCN$ (y)>
$<{}_Y^BCN$ (x)>=	$\Sigma_{k=1,4}[\ k\ {}_YW_k\ p_k^{[4]}(x)] = 4 - <{}_Y^ACN$ (x)>

Tab.A3 The four equations that define the average NN inter-ion distances ${}^{v}_{c}d$ for the four possible ion combinations in a pseudo-quaternary $A_{1-x}B_xY_yZ_{1-y}$, with *c*-centre ion, *v*-vertex ion

NN interion <d(x,y)>	Quaternary $A_{1-x}B_xY_yZ_{1-y}$
$<{}^{Z}_{A}d\ (x,y)>=$	$\{ (1-x)\ \Sigma_{k=0,3}\{ {}^{Z}_{A}d_k\ (4\text{-k}\ {}_{A}C_k) +4\ {}^{AZ}_{A}d_0 \max(0,1-{}_{A}W_k) +4\ {}^{AZ}_{A}d_4 \max[0, (k\ {}_{A}W_k -1)/(4-k)]\}\ p_k^{[4]}(y)\ \}$
	$/\{ (1-x)\ \Sigma_{k=0,3}\{(4\text{-k}\ {}_{A}C_k) +4\ \max(0,1-{}_{A}W_k) +4\ \max[0, (k\ {}_{A}W_k -1)/(4-k)]\}\ p_k^{[4]}(y)\ \}$
$<{}^{Z}_{B}d\ (x,y)>=$	$\{ x\ \Sigma_{k=1,4}\{ {}^{BZ}_{B}d_k\ (4\text{-k}\ {}_{B}C_k) +4\ {}^{BZ}_{B}d_4 \max(0,1-{}_{B}W_k) +4\ {}^{AZ}_{B}d_4 \max[0, (k\ {}_{B}W_k -1)/(4-k)]\ \}p_k^{[4]}(y)\ \}$
	$/\{ x\ \Sigma_{k=1,4}\{ (4\text{-k}\ {}_{B}C_k) +4\ \max(0,1-{}_{B}W_k) +4\ \max[0, (k\ {}_{B}W_k -1)/(4-k)]\ \}p_k^{[4]}(y)\ \}$
$<{}^{A}_{Y}d\ (x,y)>=$	$\{ y\ \Sigma_{k=0,3}\{ {}^{AY}_{Z}d_k\ (4\text{-k}\ {}_{Z}C_k) +4\ {}^{AY}_{Z}d_0 \max(0,1-{}_{Z}W_k) +4\ {}^{AY}_{Z}d_4 \max[0, (k\ {}_{Z}W_k -1)/(4-k)]\ \}p_k^{[4]}(x)\ \}$
	$/\{ y\ \Sigma_{k=0,3}\{(4\text{-k}\ {}_{Z}C_k) +4\ \max(0,1-{}_{Z}W_k) +4\ \max[0, (k\ {}_{Z}W_k -1)/(4-k)]\ \}p_k^{[4]}(x)\ \}$
$<{}^{B}_{Z}d\ (x,y)>=$	$\{ y\ \Sigma_{k=1,4}\{ {}^{BY}_{Z}d_k\ \ k\ {}_{Z}C_k\ +4\ {}^{BY}_{Z}d_4 \max(0,1-{}_{Z}W_k) +4\ {}^{BY}_{Z}d_4 \max[0, (k\ {}_{Z}W_k -1)/(4-k)]\ \}p_k^{[4]}(x)\}$
	$/\{ y\ \Sigma_{k=1,4}\{\ \ k\ {}_{Z}C_k +4\ \max(0,1-{}_{Z}W_k) +4\ \max[0, (k\ {}_{Z}W_k -1)/(4-k)]\ \}p_k^{[4]}(x)\ \}$

Table-A4. The two parallel hierarchy frequency sequences

$^{\mathbf{CdTe}}\boldsymbol{\omega}_{\mathbf{<139.5\text{-}145.6>}}$ [38, 39 p.227] $(= {}_{Cd:4Te}\omega^{Se,Te}_{0,4} = {}_{Te:4Cd}\omega^{Mn,Cd}_{0,4}) < {}_{Cd:3Te}\omega^{Se,Te}_{1,3} < {}_{Cd:2Te}\omega^{Se,Te}_{2,2} < {}_{Cd:1Te}\omega^{Se,Te}_{3,1}$
$< {}_{Cd:1Se}\omega^{Se,Te}_{1,3} < {}_{Cd:2Se}\omega^{Se,Te}_{2,2} < {}_{Cd:3Se}\omega^{Se,Te}_{3,1} < ({}_{Cd:4Se}\omega^{Se,Te}_{4,0} = {}_{Se:4Cd}\omega^{Mn,Cd}_{0,4})$
$=^{\mathbf{CdSe}}\boldsymbol{\omega}_{\mathbf{<165\square 173.5>}}$ [39 p.213, 40 p.3724], $\square < {}_{Se:3Cd}\omega^{Mn,Cd}_{1,3} < {}_{Se:2Cd}\omega^{Mn,Cd}_{2,2} < {}_{Se:1Cd}\omega^{Mn,Cd}_{3,1} <$
${}_{Se:1Mn}\omega^{Mn,Cd}_{1,3} < {}_{Se:2Mn}\omega^{Mn,Cd}_{2,2} < {}_{Se:3Mn}\omega^{Mn,Cd}_{3,1} ({}_{Se:4Mn}\omega^{Mn,Cd}_{4,0} = {}_{Mn:4Se}\omega^{Se,Te}_{4,0})$
$=^{\mathbf{MnSe}}\boldsymbol{\omega}_{\mathbf{<205\square 220>}}$ [40 p.3724]

$^{\mathbf{CdTe}}\boldsymbol{\omega}_{\mathbf{<139.5\text{-}145.6>}}$ [38, 39 p.227] $(= {}_{Te:4Cd}\omega^{Mn,Cd}_{0,4} = {}_{Cd:4Te}\omega^{Se,Te}_{0,4}) < {}_{Te:3Cd}\omega^{Mn,Cd}_{1,3} < {}_{Te:2Cd}\omega^{Mn,Cd}_{2,2} <$
${}_{Te:1Cd}\omega^{Mn,Cd}_{3,1} < {}_{Te:1Mn}\omega^{Mn,Cd}_{1,3} < {}_{Te:2Mn}\omega^{Mn,Cd}_{2,2} < {}_{Te:3Mn}\omega^{Mn,Cd}_{3,1} < ({}_{Te:4Mn}\omega^{Mn,Cd}_{4,0} = {}_{Mn:4Te}\omega^{Se,Te}_{0,4})$
$=^{\mathbf{MnTe}}\boldsymbol{\omega}_{\mathbf{<185.7\square 191.2>}}$ [38, 41 p.10938, 42 p.60] $< {}_{Mn:3Te}\omega^{Se,Te}_{1,3} < {}_{Mn:2Te}\omega^{Se,Te}_{2,2}$
$< {}_{Mn:1Te}\omega^{Se,Te}_{3,1} < {}_{Mn:1Se}\omega^{Se,Te}_{1,3} < {}_{Mn:2Se}\omega^{Se,Te}_{2,2} < {}_{Mn:3Se}\omega^{Se,Te}_{3,1} < ({}_{Mn:4Se}\omega^{Se,Te}_{4,0} = {}_{Se:4Mn}\omega^{Mn,Cd}_{4,0})$
$=^{\mathbf{MnSe}}\boldsymbol{\omega}_{\mathbf{<205\text{-}220>}}$ [40 p.3724]

Gray shade indicates the fourteen frequencies corresponding to the seven tetrahedron configurations $\{ {}_{Mn}T^{Se,Te}_{2,2}, {}_{Se}T^{Mn,Cd}_{2,2}, {}_{Se}T^{Mn,Cd}_{3,1}, {}_{Cd}T^{Se,Te}_{2,2}\ {}_{Cd}T^{Se,Te}_{3,1}, {}_{Te}T^{Mn,Cd}_{2,2}, {}_{Te}T^{Mn,Cd}_{3,1}\}$ that have evanescent probabilities of formation because of extreme site occupation preferences, as per the C_k values derived from the EXAFS data. The ranges of uncertainty for the binary configuration frequencies (taken from the literature) are indicated in this inequality sequence as subscripts and serve to define the initial fit- frequencies for the binary configurations. In a quaternary these frequencies do shift, but these values indicate the range within which the ***four***-ternary *eight*-spectrum bands should be confined, namely ≈<139-200> cm^1.

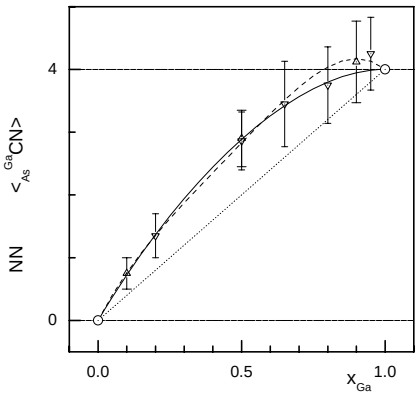

Fig.1 Occupation preferences in $Ga_xIn_{1-x}As_ySb_{1-y}$ [5]. Experimental value points: y=0.10 (triangles up), y=0.05 (triangles down). Comparison of best fit curves by the strained tetrahedron (solid curve) vs. the semi-empirical (dashed curve) model approximations and the random distribution (dotted 4x-line).

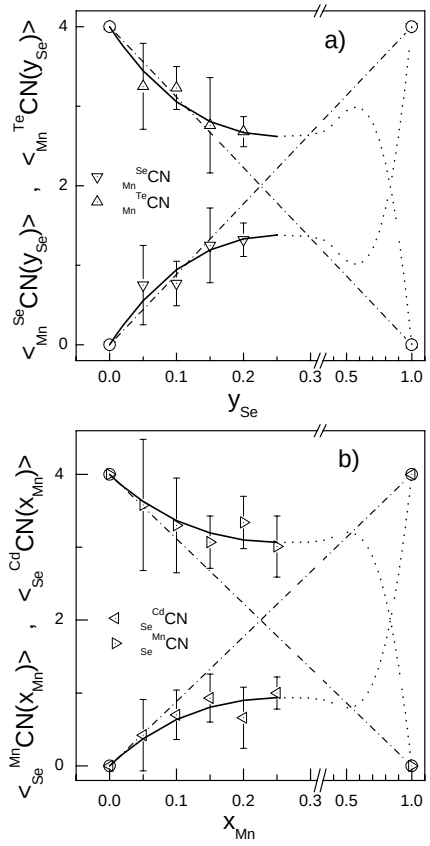

Fig.2 Analysis of $Cd_{1-x}Mn_xSe_yTe_{1-y}$ EXAFS <CN> data [4] . Experimental points (triangles); derived <CN> curves, within the sphalerite range (solid), (dotted) beyond the sphalerite range. Random limit (dash dotted): *a)* $MnSe_yTe_{1-y\ (in\ Q)}$ (Mn K-edge): $\{W_k\}_{k=1,3}=\{3.23,0,0\}$, $\{C_k\}_{k=1,3}=\{0.26,0,0\}$; *b)* $Cd_{1-x}Mn_xSe_{(in\ Q)}$ (Se K-edge): $\{W_k\}_{k=1,3}=\{2.18,0,0\}$, $\{C_k\}_{k=1,3}=\{0.61,0,0\}$.

Fig.3A Reflectivity spectra of

Fig.3B $\varepsilon_2(\omega,T)$ KK- derived spectra of

three $Cd_{1-x}Mn_xSe_yTe_{1-y}$ samples measured at different temperatures K:
a) $Cd_{0.9}Mn_{0.1}Se_{0.2}Te_{0.8}$, b) $Cd_{0.95}Mn_{0.05}Se_{0.1}Te_{0.9}$, c) $Cd_{0.85}Mn_{0.15}Se_{0.1}Te_{0.9}$.
Curves: dotted: 300 K, solid: 10 K or 30 K

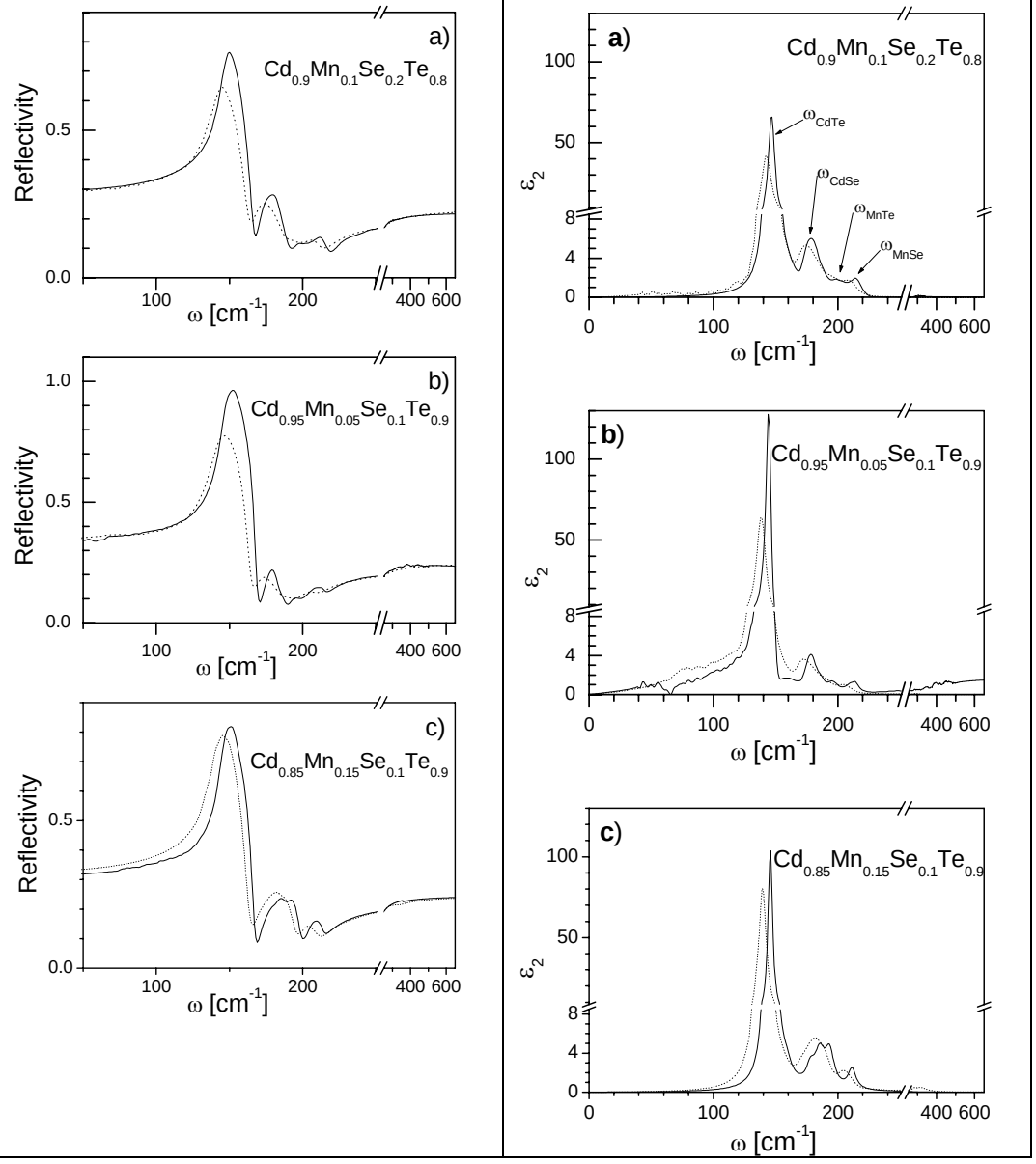

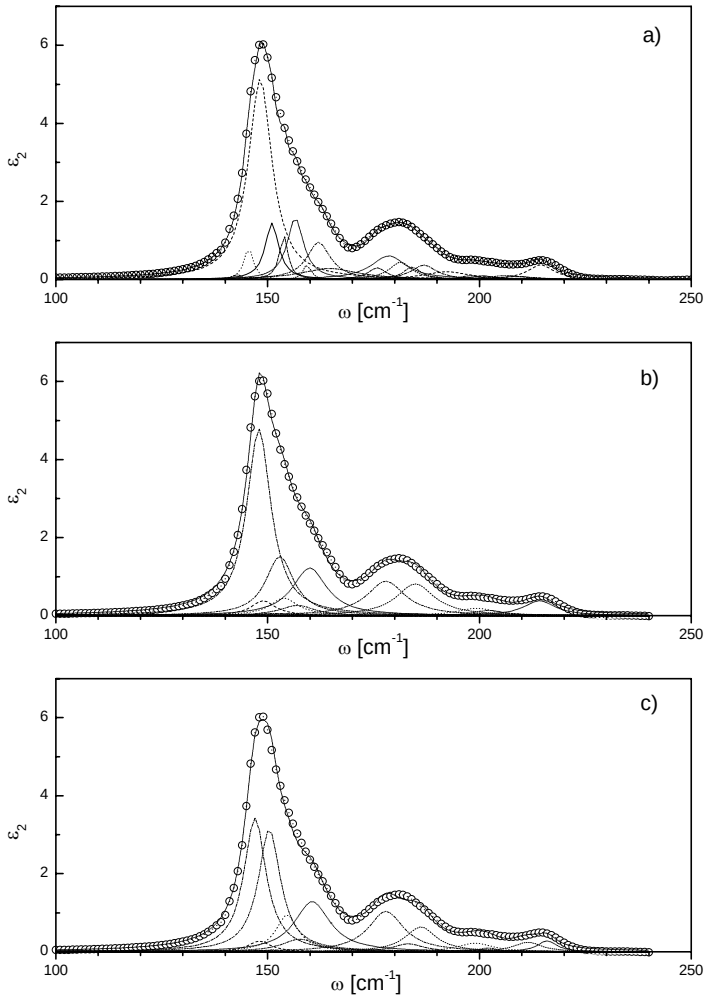

Fig.4 $\varepsilon_2(\omega,T=30\ K)$ $Cd_{0.9}Mn_{0.1}Se_{0.2}Te_{0.8}$ spectrum (circles – experimental data) and its deconvolution into component phonon lines using **a)** 32 free lines; **b)** 8+8 approximation; **c)** 4+4 approximation

Table-1 Comparison of NN values for $GaInAs_{(as\ T)}$ [20,1] with those of $GaInAs_{(in\ Q)}$. The last line (in *italics*) reports data obtained using the semi-empirical approach [7]

$GaInAs_ySb_{1-y}$	${}_cT_k$	${}_{As}W_k$			${}_{As}C_k$			${}^{Ga}_{As}d_k$			${}^{In}_{As}d_k$ [Å]		
	c=As	k=1	2	3	1	2	3	k=1	2	3	1	2	3
$GaInAs_{(in\ Q)}$													
y_{As} =0.05		1.88	1.54	1.32				2.81	2.45	-	2.66	2.53	-
x_{Ga}={0.2, 0.5, 0.65, 0.8, 0.95}					0.71	0.46	0.05						
y_{As} =0.10		1.93	1.59	1.33				2.84	2.34	-	2.65	2.49	-
x_{Ga}={0.1, 0.5, 0.9}					0.69	0.41	0						
both together		1.89	1.56	1.33	0.70	0.44	0	**2.80**	**2.44**	**-**	**2.65**	**2.52**	**-**
$GaInAs_{(as\ T)}$		1.05	0.25	0.58	0.85	0.25	0.58	2.49	2.42	2.48	2.59	2.60	2.61
Semi-empiric model		*2.19*	*1.07*	*1.64*	*0.60*	*0.93*	*0*						

Table-2 $Cd_{1-x}Mn_xSe_yTe_{1-y}$: comparison of NN values for $CdMnTe_{(as\ T)}$ [20,1] with those of $GaInAs_{(in\ Q)}$. Last raw (in italics): data obtained using the semi-empirical approach [7]

Ternary	${}_cT_k$	${}_cW_k$			${}_cC_k$		
	c	k=1	2	3	k=1	2	3
MnSeTe$_{(in\ Q)}$		3.23		0			0
	Mn	3.22		0.20			0.40
		3.23	0	0.40	0.26	0	**0.20**
CdMn**Se**$_{(in\ Q)}$	*Se*	2.18	0	1.33	0.54	0	0
CdSeTe$_{(in\ Q)}$	*Cd*	2.38	0	1.33	0.54	0	0
CdMn**Te**$_{(in\ Q)}$	*Te*	3.23	0	0	0.26	0	0
CdMn**Te**$_{(as\ T)}$		*0.68*	*1.33*	*0*	*0.68*	*0.67*	*0*
CdMnSeTe$_{(as\ T)}$ *Semi-empiric model*		*1.9*	*1.6*	*1.3*	*0.70*	*0.40*	*0*

Table-3 Comparison of σ^2 of best-fits of 8+8 and 4+4 approximations for all nine $Cd_{1-x}Mn_xSe_yTe_{1-y}$ spectra, with different temperatures

Sample	T K	σ^2_{8+8}	σ^2_{4+4}
x=0.1, y=0.2	30	4.1E-03	4.0E-03
x=0.15, y=0.1	10	1.9E-01	2.4E-01
x=0.05, y=0.1	10	1.0E-02	9.1E-02
x=0.05, y=0.1	300	5.3E-03	3.2E-02
x=0.15, y=0.1	300	6.5E-03	3.0E-02
x=0.1, y=0.2	300	2.3E-03	4.4E-03

7 ACKNOWLEDGEMENTS

Part of the work was supported by the EU TARI-project contract HPRI-CT-1999-00088.

8 REFERENCES

[1] B.V.Robouch, A.Kisiel, J.Konior, *J.Alloys Compounds* **339**, 1 (2002)

[2] E.Oh, R.G.Alonso, I.Miotkowski, A.K.Ramdas, *PhysRevB* **45**(1992)10934

[3] J.Polit, R.Hus ,E.M. Sheregii, E.Sciesinska , J.Sciesinski, B.V.Robouch, A. Kisiel, *Far Infrared Spectra in the tetrahedral Quaternary Alloys*, (Proc. NGS 10) Proc. 10th International Conf. on Narrow Gap Semiconductors and Related Small Energy Phenomena, Physics and Applications, Japan Advanced Institute of Science and Technology and Kanazawa Kokusai May 27-31, 2001, Ishikawa, Japan, (IPAP) The Institute of Pure and Applied Physics Conf.Series2 pp.155-157.

[4] A.Kisiel, J.Łażewski, M.Zimnal-Starnawska, E.Burattini, A.Mycielski, *Acta Phys.Polonica A* **90** 1032 (1996); Idem, *J. de Physique IV, France* **7 C2** 1197 (1997)

[5] Sh.M.Islam, B.A.Bunker, *Physics Letters A* **156** 247 (1991)

[6] Q.Lu, B.A.Bunker, H.Luo, A.J.Kropf, K.M.Kemner, J.K.Furdyna, *Phys.Rev.B,* **55** 9910 (1997)

[7] B.V.Robouch, A.Kisiel, Acta Phys.Pol.A 94, 497 (1998) ; Idem, *J. Alloys Compounds* 286, 80 (1999) ; Idem, Synchrotron Radiation Studies of Materials, Proc. 5th Polish National Symp. of Synchrotron Radiation Users, Warsaw 1999, Ed. J.Gronkowski, M.Lefeld-Sosnowska Ed. office Institute of Experimental Physics, Warsaw Univ., Warsaw 1999 p. 207

[8] H.W.Verleur and A.S.Barker, *Phys.Rev*. **149** 715 (1966)

[9] H.W.Verleur and A.S.Barker, *Phys.Rev*. **155** 750 (1967)

[10] B.V.Robouch, A.Kisiel, E.M.Sheregii, *Phys. Rev.B* **64**, 73204 (2001)

[11] B.V.Robouch, E.M.Sheregii, A.Kisiel, *Fiz. Nizkikh Temp: Low Temp. Phys.* **30**, 1225 (2004)

[12] B.V.Robouch, E.M.Sheregii, A.Kisiel, *phys .stat. sol.*(c) **1**, 3015 (2004)

[13] B.V.Robouch, A.Kisiel, J.Konior, *J. Alloys Compounds* **340** ,13 (2002)

[14] B.V.Robouch, E.Burattini, A.Kisiel, A.L.Suvorov, A.G.Zaluzhnyi, *J. Alloys Compounds* **359**, 73-78 (2003)

[15] R. A. Mayanovic, W.-F. Pong, B. A. Bunker, *Phys. Rev. B*, **42** (1990-I) 11174

[16] A. Balzarotti, N. Motta, A. Kisiel, M. Zimnal-Starnawska, M. T. Czyzyk, M. Podgórny, *Phys. Rev. B* **31** (1985) 7526;

- A. Balzarotti, M. T. Czyzyk, A. Kisiel, N. Motta, M. Podgórny, M. Zimnal-Starnawska, *Phys. Rev. B*, **30** (1984) 2295

[17] N. Motta, A.Balzarotti, P. Letardi, *J.Crystal Growth* **72** (1985) 205-209; Idem, *Solid State Commun*. **53** (1985) 1985

- A. Balzarotti, M. T. Czyzyk, A. Kisiel, P. Letardi, N. Motta, M. Podgórny, M. Zimnal-Starnawska, *Festkörperprobleme* XXV (1985) 689

[18] K.E.Miyano, J.C.Woicik, L.H.Robins, C.E.Bouldin, D.K.Wickenden, *Appl.Phys.Lett.* 70 (1997) 2108

[19] Z. Wu, K. Lu, Y. Wang, J. Dong, H. Li, Ch. Li, Zh. Fang, *Phys. Rev. B* **48** (1993) 8694-8700

[20] J. C. Mikkelsen and J. B. Boyce, *Phys. Rev. Lett.* **49** (1982) 1412; Idem, J *Phys. Rev. B*, **28** (1983) 7130

[21] A.Marbeuf, D.Ballutaud, R;Triboulet, H.Dexpert, P.Lagarde, Y.Marfaine, *J.Phys.Chem.Solids* **50** (1989) 975

[22] M. Zimnal-Starnawska, J. Lazewski, A. Kisiel, *Acta Phys. Pol.* **86** (1994) 763-766 .

[23] R. Iwanowski, K. Lawniczak-Jablonska, I. Winter, J. Hormes, *Solid State Commun.* **97** (1996) 879

[24] J. Lazewski, M. Zimnal-Starnawska, A. Kisiel, F. Boscherini, S. Pascarelli, W. Giriat, *Phys Stat. Sol. (b)* **197** (1996) 7-12

[25] W.-F. Pong, R. A. Mayanovic, B. A. Bunker, J. K. Furdyna, U. Debska, *Phys. Rev. B,* **41** (1990-II) 8440

[26] A. Bunker, *J. Vac. Sci. Technol.* , **A5** (1987) 3003

[27] N. Happo, H. Sato, T. Mihara, S. Hosokawa, Y. Ueda, M. Taniguchi, *J. Phys. Condens. Matter* **8** (1996) 4315

[28] S.P.Kozyrev, L.K.Vodopyanov, R.Tribulet, *Solid State Commun.***45** 383 (1983)

[29] S.Perkowitz, L.S.Kim, P.Becla, *Phys.Rev.***43** 6598 (1991)

[30] S.Perkowitz, L.S.Kim,, Z.C.Feng, P.Becla, *Phys.Rev.***42** 1455 (1990)

[31] N.Romcevic, M.Romcevic, A.Golubovic, Le Van Khoi, A.Mcielski, D.Jovanovic, D.Stojanovic, S.Nikolic, S.Duric, *J.Alloys Compounds* 397(2005) 52

[32] P.A. Lee, P.H. Citrin, P. Eisenberger and B. M. Kincaid, *Rev. Mod. Phys.* **93**, 769 (1981)

[33] B.K. Teo, *EXAFS:Basic Principles and Data Analysis*, Springer Verlag, 1986

[34] P.A. Lee, P.H. Citrin, P. Eisenberger, B.M. Kincaid , *Rev. Mod. Phys.* **53,** 769 (1981).

[35] S.Chebab, G.Lamarche, A.Manoogian, J.C.Wooley, *J.Magn.Magn.Mater,* 59 (1986) 105

[36] A. Mycielski, W. Dobrowolski, A. Szdkowski, et al., Proceeding of the 20th ICPS Thessaloniki, Greece, 1990 (Edited by E.M. Anastassakis & J.D. Joannopoulos) Vol. 3, p. 1827, World Scientific, (1990) , p. 702.

[37] M. Cestelli Guidi, M. Piccinini, A. Marcelli, A. Nucara, P. Calvani, E. Burattini, "Optical performances of SINBAD, the Synchrotron Infrared Beamline At DAΦNE", *Journal of the Optical Society of America*, (in press), (2005)

[38] J.M.Wrobel, B.P.Clayman, P.Becla, R.Sudharsanan, S.Perkowitz, *J.Appl.Phys.* **64** (1988) 310

[39] Landolt Bornstein vol.**17b**, Ed.K-H.Hellwege, Springer-Verlag, Berlin 1982

[40] R.G.Alonso, E-K.Suh, A.K.Ramdas, N.Samarth, H.Luo, J.K.Furdyna, *PhysRevB* **40**(1989)3720

[41] E.Oh, R.G.Alonso, I.Miotkowski, A.K.Ramdas, *PhysRevB* **45**(1992)10934

[42] G.G.Tarasov, Yu.I.Mazur, W.Hoerstel, W.T.Masselink, *J.Alloys & Compounds* **371** (2004) 58